ADVANCED OPTICAL MATERIALS
www.advopticalmat.de

PEA_2SnI_4 Perovskite Thin Films for Photonics: Linear and Nonlinear Optical Properties and Waveguided Photoluminescence

Isaac Suárez, Jesús Sánchez-Díaz, Hamid Pashaei Adl, Iván Mora-Seró,* and Juan P Martínez-Pastor**

In this work, 2D PEA_2SnI_4 (PEA: 2-phenylethanaminium) perovskite thin films, formed with the reducing agent $NaBH_4$ to control the Sn^{+4} defects are investigated. Optical characterization of the films reveals idoneous properties for the development of photon sources, particularly an extraordinarily high absorption coefficient at the exciton resonance > 10 μm^{-1}, the ability to enhance the light-matter interaction due to the high refractive index. These linear optical properties are complemented with impressive nonlinear optical characteristics, involving a giant nonlinear absorption β = 7–10 cm MW^{-1} and a remarkably high nonlinear refractive coefficient, n_2 = 1.5–4 cm^2 GW^{-1}. The integration of PEA_2SnI_4 films into rigid and flexible waveguides further enhances the generation of waveguided photoluminescence (PL), which is also obtained under the two-photon absorption mechanism. The efficient generation of PL is validated by the reabsorption effect, resulting in the propagation of recycled photons over distances longer than 3 mm with an increased effective lifetime from 3 to 8.5 ns. These findings pave the way for the development of novel photonic functionalities based on these innovative low-dimensional semiconductors.

1. Introduction

During the last decades, the topic of semiconducting metal halide perovskites (MHPs) has attracted enormous attention in all the optoelectronic community around the world.[1,2] Fabricated under low-cost and straightforward methods, MHPs exhibit extremely high light absorption and emission efficiencies, bandgap tunability, and high carrier diffusion lengths, among other outstanding properties[3] that enabled the implementation of cutting-edge devices in several areas, such as solar cells,[4] photodetectors[5] or optical sources.[6] In this way, the field of MHPs has recently advanced toward the investigation of Sn-based compounds, which represent a less toxic alternative to the more developed Pb-containing perovskites.[7,8] Although Sn-perovskite thin films have faced challenges with oxidation under ambient conditions, the significant effort carried out by the scientific community during the last years has led to the development of relatively more stable and reliable compounds. Nowadays, a panoply of Sn-based perovskite devices is available following the footsteps of their Pb-containing counterparts in terms of performance. Among other devices, Sn-perovskites have successfully demonstrated good properties in photodetectors,[9,10] transistors,[11] light emitting diodes (LEDs),[12–14] solar cells[15,16] or lasers.[17–20] This progress not only underscores the versatility and potential of MHPs but also paves the road for environmentally friendly and sustainable optoelectronic technologies.

In this context, the synthesis of Sn-perovskites as 2D or near-2D multilayered MHP semiconductors, i.e., the Ruddlesden–Popper phases, represents a new advance in the field of perovskites. 2D Ruddlesden–Popper multilayered perovskites are the organic equivalent of epitaxial multi-quantum well structures and consist of inorganic layers with high dielectric constant spaced by organic cation layers with low dielectric constant.[21] Then, the number, thickness, and dielectric constant of each layer introduce alternative degrees of freedom to tune the optoelectronic properties of the perovskite film.[22,23] Compared with their 3D counterpart, 2D perovskites demonstrate very large exciton binding energies,[23] optical anisotropy where the emission dipole is polarized to a preferred direction,[24] the formation of edge estates at the grain boundaries which enables the dissociation of excitons into free carriers,[25] a larger color gamut and

I. Suárez, H. Pashaei Adl, J. P Martínez-Pastor
UMDO
Instituto de Ciencia de los Materiales
Universidad de Valencia
Valencia 46980, Spain
E-mail: isaac.suarez@uv.es; juan.mtnez.pastor@uv.es
J. Sánchez-Díaz, I. Mora-Seró
Institute of Advanced Materials (INAM)
Universitat Jaume I
Castelló de la Plana, Castelló 12006, Spain
E-mail: sero@uji.es

The ORCID identification number(s) for the author(s) of this article can be found under https://doi.org/10.1002/adom.202402372

DOI: 10.1002/adom.202402372

efficiency in the emission spectra,[26] or a stronger nonlinear response due to the exciton confinement effects.[27] Consequently, 2D perovskites exhibit enhanced radiative lifetime, stability, and purity of emission, which are excellent qualities for LEDs or displays.[28–30] In the case of Sn-perovskites, the synthesis on a pure iodine-based 2D morphology is particularly beneficial to generate red light, because of the smaller bandgap compared to their Pb counterparts, which results in an efficient pure red emission at 630–640 nm at room temperature without the need of mixing halides.[31,32] At these conditions, 2D Sn-perovskites are unique ecofriendly materials for red LEDs providing high emission efficiency and color purity.[33,34] Among the different organic cations explored for 2D Sn-perovskites, phenylethylammonium (PEA) significantly enhances the quantum yield (QY) of emission and improves the crystallization.[35] Moreover, incorporating antioxidant additives into the precursors of PEA_2SnX_4 (X = Br, I) reduces the hole concentration appearing from Sn-vacancies and improves the stability of the film.[13,34] Consequently, PEA_2SnI_4 has been proven effective in the implementation of LEDs in both rigid and flexible substrates,[13,34] and also in other optoelectronic functionalities such as photodetection,[36] sensing[37] and in the generation of optical gain.[38,39]

To further optimize these materials for technological applications, it is essential to thoroughly investigate their optical properties and understand how light propagates through the films. This analysis will provide the required inputs to improve the current technology or to design more complex optoelectronic and photonic devices. In this manuscript, the linear and nonlinear optical properties of PEA_2SnI_4 thin films are extensively characterized and applied in waveguided photoluminescence (PL) in the film plane. First, the determination of the optical constants, i.e., refractive index, indicates a strong excitation coefficient, $k \approx 1$, at the excitonic resonance together with a refractive index between $n \approx 2.3$ and $n \approx 2.6$ at the PL region (600–700 nm), which results on a high enough index contrast with respect to commercial substrates (SiO_2, glass or polymers with $n \approx 1.5$), as the basis to develop functionalities based on the confinement of light. In particular, the PEA_2SnI_4 films integrated in both rigid SiO_2/Si and flexible polyethylene terephthalate (PET) substrates exhibit an efficient generation and propagation of PL when the device is optically excited above the bandgap. Moreover, the same films exhibited guided PL under infrared optical pumping, indicating that the semiconductor under study is a suitable nonlinear medium, particularly under two-photon absorption (TPA) conditions.[40] Furthermore, the films studied under nanosecond (ns) pulses at 1064 nm revealed promising third-order nonlinear optic properties a high refractive, n_2 = 1.5–4 $cm^2\ GW^{-1}$ and absorptive, β = 7–10 $cm\ MW^{-1}$ coefficients. Nonlinear coefficients of Sn-perovskites are addressed in a few publications, mainly dealing with nanocrystals in solution or platelets.[41–43] Finally, the planar waveguide configuration allows the analysis of the propagated PL along several millimeters. Interestingly, the high efficiency of emission and absorption of the PEA_2SnI_4 thin film together with the strong light-matter interaction provided by the waveguide, resulted in an efficient photon recycling effect that boosts the PL signal by several cycles of photon emission and absorption. In particular, we measured an increase in the effective decay time from 3 to 12 ns, which provides an enhancement of 20% on the emitted PL. This is an important result that improves our previous findings in films of $CsPbBr_3$ nanocrystals[44] and, to the best of our knowledge, first demonstrated for PEA_2SnI_4. All these insights are necessary ingredients to better understand the physical properties of PEA_2SnI_4 and with it to pave the road for more efficient red emitters or to develop additional nonlinear photonic functionalities based on these novel semiconductor materials.

2. Characterization of Linear Optical Properties

2.1. Absorption, Refractive Index and Photoluminescence Emission

PEA_2SnI_4 films were spin-coated on the appropriate substrate following the procedure described in the methods section and detailed elsewhere.[13] The structural characterization in samples of PEA_2SnI_4 without and with additives (SnF_2, $NaBH_4$, and SnF_2+$NaBH_4$) indicates that the films are formed by compact polycrystalline grains and present good homogeneity, see Figure S1 (Supporting Information). Figure S2 (Supporting Information) presents the X-ray diffraction (XRD) pattern of these films, showing their high crystallinity and uniformity. The presence of only (00n) diffracted peaks suggests the parallel orientation of the perovskite planes with respect to the substrates, which is very characteristic of a 2D perovskite,[1–3] showing repetitive XRD peaks with the interval of ≈5.41°, which corresponds to the interlayer distance of the inorganic layers ≈1.63 nm calculated using the Bragg's equation (see Supporting Information). As previously reported,[13] the quality of the PEA_2SnI_4 films is significantly enhanced with the participation of the indicated additives. In particular, among the four combinations, the PEA_2SnI_4 films prepared with the $NaBH_4$ additive were chosen in the present work, because they presented better stability under light illumination together with minimized surface pinholes, see the SEM image in Figure S1c (Supporting Information).

The absorption coefficient (α) of the PEA_2SnI_4:$NaBH_4$ is obtained here from the transmittance and reflectance spectra following the procedure detailed elsewhere.[45,46] The absorption spectrum of the films spin-coated on a borosilicate substrate, see **Figure 1a** (solid green line), shows an exciton resonance close to 600 nm with a remarkably high absorption coefficient (>15 μm^{-1}). This spectrum agrees with those reported in the literature[13,37,47] and is similar to that measured on films deposited on flexible Polyethylene Terephthalate (PET), see Figure S3 (Supporting Information). It is worth mentioning that this absorption coefficient at the exciton resonance exceeds that measured in other perovskites, such as polycrystalline $FASnI_3$[18] and $MAPbI_3$ (MA = methylammonium)[45] thin films, or close-packed films of $CsPbBr_3$ and $CsPbI_3$ nanocrystals,[48] where α is typically ≈1 μm^{-1}. This feature indicates that the perovskite thin films studied here mainly concentrate on the oscillator strength at the exciton ground state, corroborating their 2D character.[49] The spontaneous emission or PL spectrum of a PEA_2SnI_4:$NaBH_4$ film deposited on borosilicate is shown in Figure 1a (red shaded area) and consists of a near Gaussian shape centered at 631 nm with a full width at half maximum (FWHM) of ≈25–30 nm, which also agrees with the spectra found in the literature.[13,34,37,47] Again, a similar PL spectrum with slightly larger FWHM is

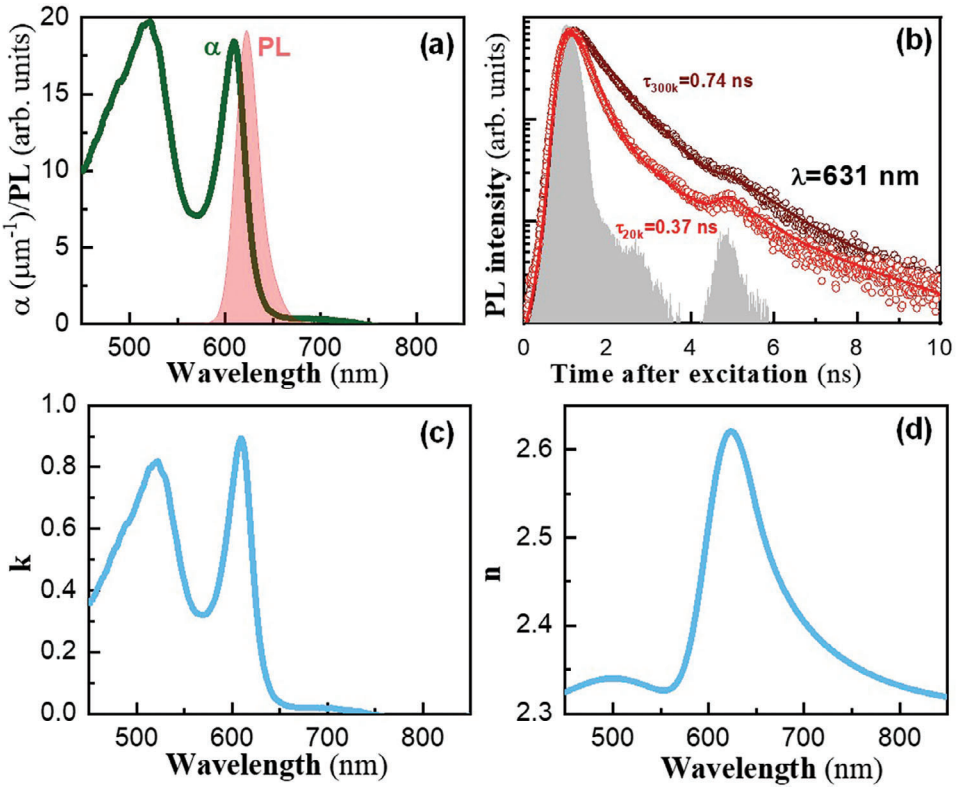

Figure 1. PL, absorption, and linear optical properties of the $PEA_2SnI_{4\ are}$ used in this work. a) Absorption (solid green line) and PL (red area). b) TRPL at room temperature (brown) and 20 K (red). Symbols, solid lines, and grey areas correspond to the experimental data, fitting, and system response, respectively. c) The imaginary part of the refractive index. d) The real part of the refractive index.

obtained in films deposited on flexible PET (Figure S3, Supporting Information). The TRPL spectrum at the PL peak wavelength exhibits a biexponential decay, $A{\cdot}e^{-t/\tau 1}+B{\cdot}e^{-t/\tau 2}$, with short, τ_1 = 0.74 ns, and long, τ_2 = 2.5 ns, times at room temperature, see brown symbols in **Figure** 2b, which are attributed to exciton recombination with the participation of shallow levels at room temperature, respectively.[34] The TRPL carried out at longer emission wavelengths within the emission (641 nm) yields a similar decay, with τ_1 = 0.71 ns (Figure S4, Supporting Information). The TRPL at 20 K (red symbols in Figure 2b) yields a decrease of the short radiative time τ_1 = 0.37 ns, as expected in a 2D semiconductor. The PL QY measured at room temperature with an integrated sphere was ≈1.2%. This means that the measured decay time in the PL transient at room temperature is practically defined by nonradiative channels with τ_{nr} = 0.75 ns, possibly associated with defects at grain boundaries and film surface, whereas the expected radiative time would be τ_r = 61.7 ns.

To properly design a photonic device based on the PEA_2SnI_4 thin film is mandatory to determine the optical constants, i.e., the complex refractive index (n-ik), at the operation wavelengths. For this purpose, we carried out the procedure described in Section 4 of the Supporting Information, see also Figure S5 (Supporting Information). Briefly, the imaginary part of the refractive index is first fixed from the absorption spectrum ($k = \alpha{\cdot}\lambda/4{\cdot}\pi$, where λ is the wavelength), and the resulting extinction coefficient (k) is plotted in Figure 1c. As expected from the absorption spectrum shown in Figure 1a, the films show a remarkably high k≈1 at the excitonic resonance revealing a strong oscillator strength.[49] Then, the real part of the refractive index, n, is obtained, see Figure 1d, from the best fitting of the reflectivity under normal incidence of the film deposited on the borosilicate substrate with a multilayer algorithm, see Figure S5 (Supporting Information).[50] At these conditions, n shows an inflection point at the excitonic resonance characteristic of a dipolar transition[49] and falls between 2.3 and 2.65 at emission wavelengths (600–700 nm). The wavelength variation of real and imaginary refractive indices obtained here is very similar to that reported in the literature from ellipsometry.[37] Of course, the dispersion curve for n presented here in Figure 1d corresponds to the in-plane refractive index. Although, given the 2D character of the perovskite semiconductor under study, a slightly different refractive index is expected in the out-plane direction,[51] we believe that under the range of thicknesses used in this work (80–200 nm), the in-plane n is dominant for practical applications.

2.2. Nonlinear Optical Properties

To fully understand the benefits of the PEA_2SnI_4 thin films as a photonic material, it is interesting to characterize the third-order nonlinear optical constants, which would allow more complex and important applications of this material for telecom technologies, such as all-optical switching, quantum communications, data storage, frequency combs, etc.[40] All centrosymmetric

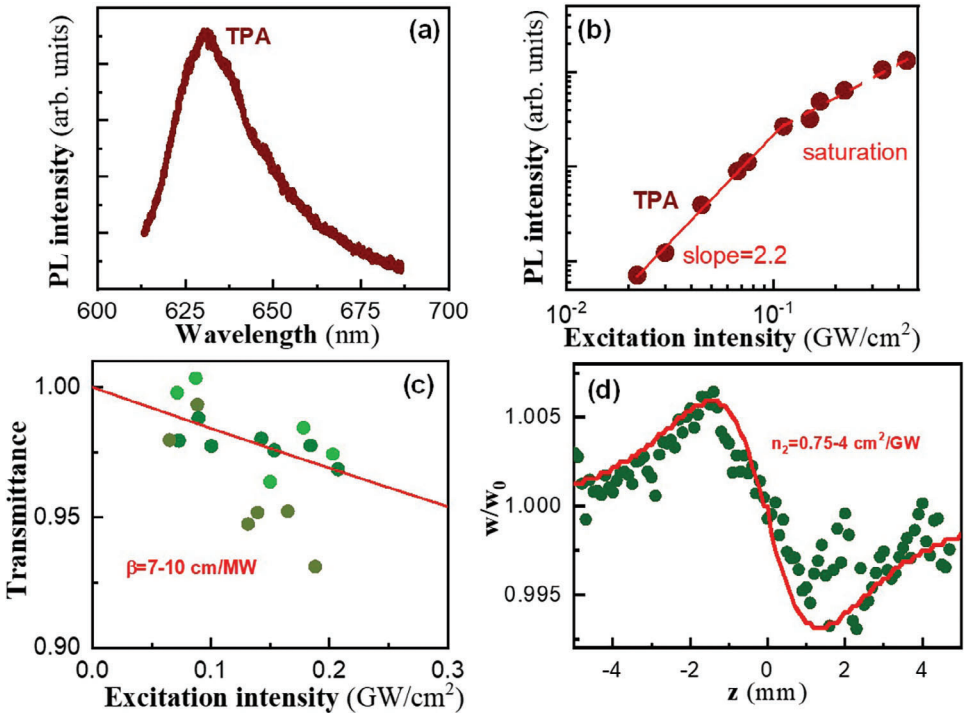

Figure 2. Nonlinear characterization of PEA_2SnI_4 thin films. a) PL under infrared TPA pumping at 1064 nm. b) Log–log plot of the intensity of PL versus excitation at 1064 nm. T c) Transmittance of a 1064 nm beam through the PEA_2SnI_4 versus the excitation fluence. The colors indicate three different measurement points in the sample. d) Z-scan characterization. Symbols correspond to the experimental data and solid lines to the fitting.

crystals experience a nonlinear change of the refractive index (Δn) with the intensity of the incident beam (I) given by:

$$\Delta n = n_2 \cdot I - i \cdot \frac{\lambda}{4 \cdot \pi} \cdot \beta \cdot I \quad (1)$$

where n_2 and β are the refractive and absorptive nonlinear coefficients, respectively. In most crystals, however, the nonlinear optical coefficients, n_2 and β, are usually so low that extremely high-intensity pulses are required to produce an observable Δn. Nevertheless, the nonlinear characterization carried out in different MHPs suggests that this family of semiconductors presents outstanding nonlinear coefficients that exceed that of silicon or GaAs.[40,52] Furthermore, the excitonic confinement in the 2D perovskites would further enhance the nonlinear properties in comparison to their 3D counterparts, leading to giant n_2 and β coefficients.[27,53–55]

First of all, MHPs are characterized by efficient absorption under infrared pumping.[56] This effect is known as TPA and is based on the promotion of electrons from the valence to the conduction band via virtual states induced by the simultaneous absorption of two photons. Under 1064 nm pulsed laser excitation, the sum of two pump photons of energy 1.165 eV is sufficient to overcome the bandgap of the material at ≈2 eV and promote the TPA mechanism. At these conditions, the 2D PEA_2SnI_4 semiconductor exhibits a bright generation of PL under TPA conditions with a spectrum centered at ≈630 nm with a FWHM 35 nm, as shown in Figure 2a (brown line), which is similar to standard PL shown in Figure 1a. The dependence of the PL intensity (I_{PL}) as a function of the excitation fluence (I) exhibits a quadratic variation $I_{PL} \propto I^2$ characteristic of the TPA nonlinear process, see the log–log plot in Figure 2b. The saturation observed above 0.2 GW cm^{-2} can be attributed to thermal effects or a certain deterioration of the sample under laser excitation at ambient conditions. The β parameter associated with the TPA mechanism is obtained by measuring the transmittance (T) of a 1064 nm beam through the PEA_2SnI_4 thin films as a function of I, see Figure 2c, and fitting the experimental data, symbols in Figure 2c, with the characteristic equation for TPA, $dI/dz = -\beta \cdot I^2$,[55,57] A nonlinear coefficient β = 7–10 fits cm MW^{-1} reasonably well with the experimental data, see red line in Figure 2c, where the variations observed are less than 5%. This measurement was carried out at three different points, represented by the three colors in the figure, to verify the accuracy of determining this parameter. The value of nonlinear coefficients depends on different factors, such as the excitation wavelength (or the ratio of excitation wavelength versus bandgap), the pulse size, or the dimensionality of the semiconductor. In this way, the average value of β overcomes the values measured under similar excitation conditions (1 ns pulses at 1064 nm) in PbX_3 (X = Br, I) thin films (0.3–15 cm MW^{-1}),[52] in solutions containing $CsPbX_3$ nanocrystals (0.3–1.1·10^{-3} cm MW^{-1}),[52] or comparable to solutions containing Cs_2SnI_6 nanocrystals (0.08–0.1 cm MW^{-1}). Such a big β coefficient can be explained by the enhancement of the nonlinear response by excitonic confinement effects, which has been already demonstrated in Pb Ruddlesden-Popper perovskite thin films.[27] Accordingly, the value of β obtained here for PEA_2SnI_4 is close to that reported for $CsSnBr_3$ nanoplatelets (23 cm MW^{-1}) measured under picosecond (ps) pulses at 1064 nm, and below the values measured for PEA_2PbI_4 flakes (211.5 cm MW^{-1})[55]

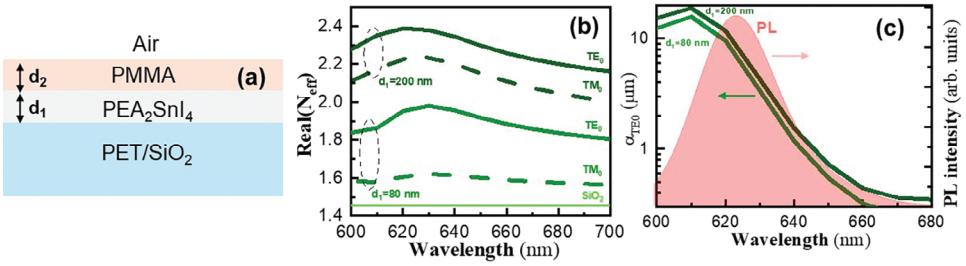

Figure 3. a) Waveguide structure. b) The real part of the effective of the TE_0 (solid lines) and TM_0 (dash lines) modes in waveguides with d_1 = 80–200 nm and d_1 = 1 µm. c) Absorption coefficient of the TE_0 (TM_0 provides similar results) in waveguides with d_1 = 80–200 nm and d_2 = 1 µm. The red area represents the PL.

or 2D perovskite heterostructures (44 cm MW^{-1}),[57] possibly due to the better crystallinity and hence absence of losses in the polycrystalline grains. At these conditions, PEA_2SnI_4 thin films are promising media in applications based on TPA. Examples include biological imaging, absorption saturation, and optical sources, among others.

In agreement with the giant nonlinear absorption coefficient, PEA_2SnI_4 thin films also present a remarkable nonlinear refractive index derived from the excitonic confinement.[27] The coefficient n_2 is studied here at the same excitation conditions (1064 nm, 1 ns, 20 kHz) with the image Z-scan set-up described elsewhere.[52] Figure 2d shows a representative characterization of a ≈100 nm PEA_2SnI_4 thin film deposited on borosilicate and fitted with the model described in ref. [52] solid line in Figure 2d. In particular, a Kerr coefficient n_2 as high as 0.75–4 cm^2 GW^{-1} is deduced from the different experimental data, which is similar to that found in polycrystalline thin films of NH_3MAPbX_3 perovskites measured with the same experimental set-up.[52] In the case of Ruddlesden–Popper perovskites, the determination of the coefficient n_2 is reduced to few publications, where values between $2.88{\cdot}10^{-5}$ cm^2 GW^{-1} and $2.88{\cdot}10^{-3}$ cm^2 GW^{-1} were deduced from measurements under femtosecond pulses.[27,54] Therefore, PEA_2SnI_4 films can be also promising as self-focusing media, which could be eventually used for harmonic generation, soliton formation, or mixing waves, among other applications.[40]

2.3. Application in Optical Waveguides

Based on the analysis carried out in the previous sections, the 2D PEA_2SnI_4 thin films possess the required qualities needed for developing photonic applications and optical sources based on guided light: i) high refractive index to confine and propagate light, ii) high efficiency of absorption and emission to generate PL, iii) exceptional nonlinear parameters to design more sophisticated functionalities. In this way, PEA_2SnI_4 thin films (thickness d_1 = 80–200 nm) were used to form planar waveguides by simply covering the film with a Poly(methyl methacrylate) (PMMA) cladding layer (thickness d_2 = 1 µm) onto both rigid SiO_2(2 µm)/Si and flexible PET substrates, as illustrated in **Figure 3a**. The waveguides were analyzed by using the multilayer algorithm to obtain the propagation modes and their effective refractive indices, as explained elsewhere.[50] As we demonstrated for similar waveguides containing polycrystallineMAPbI$_3$ thin films,[58] the high refractive index contrast between the perovskite film compared to the surrounding layers results in propagation modes highly confined in the semiconductor film in both transverse electric (TE) and transverse magnetic (TM) polarizations. For the range of thicknesses used in this work, d_1 = 80–200 nm, the real part of the effective refractive indices (N_{eff}) at the PL window (600–680 nm) lays between Real(N_{eff}) = 1.8–2.4 and Real(N_{eff}) = 1.6–2.0 for TE_0 and TM_0 modes, respectively, see Figure 3b for SiO_2/Si substrate. Waveguides of $FASnI_3$ (FA - formamidinium) films deposited on flexible PET exhibit similar N_{eff} values, because these substrates also have a small refractive index (n = 1.5), similar to SiO_2.[18] Such high Real(N_{eff}) values will lead to strong confinement of the modes in the active perovskite layer enhancing the efficiency of absorption and emission. Indeed, the attenuation of the fundamental modes at the PL peak wavelength is as high as 10 μm^{-1}, as observed Figure 3c (continuous lines for absorption and red shaded area for PL).

2.4. Pumping and PL Waveguiding Under OPA and TPA Conditions

The waveguides were first analyzed by end-fire coupling an excitation laser beam from the input edge of the sample and collecting waveguided PL, see **Figure 4a**. A similar set-up was used to demonstrate amplified spontaneous emission (ASE) with $MAPbI_3$ and $FASnI_3$ films in similar waveguide structures integrated in rigid and flexible substrates.[18,59] Particularly, the system is based on the propagation of the excitation beam along the whole length of the waveguide through the PMMA cladding modes and the strong light-matter interaction of the fundamental TE_0/TM_0 modes within the semiconductor.[58] Figure 4b presents representative results of waveguided PL studied on a rigid substrate under 2 ps pulsed laser excitation at 532 nm, i.e., One Photon Absorption (OPA) conditions because the excitation photon energy is above the bandgap of PEA_2SnI_4. The PL spectrum is composed of two emission bands located at 626 and 646 nm, as observed in Figure 4b (greenish color lines under different excitation powers). As postulated for 3D perovskites[58] and 2D 2-thiopheneethylammonium tin(II) iodide, TEA_2SnI_4 (TEA - thiopheneethylammonium) perovskite,[60] two-band PL spectra can arise by the contribution of intrinsic and trapped excitons in grain boundaries or maybe grains subjected to higher strain leading to lower energy excitonic states, as can be the case here. In

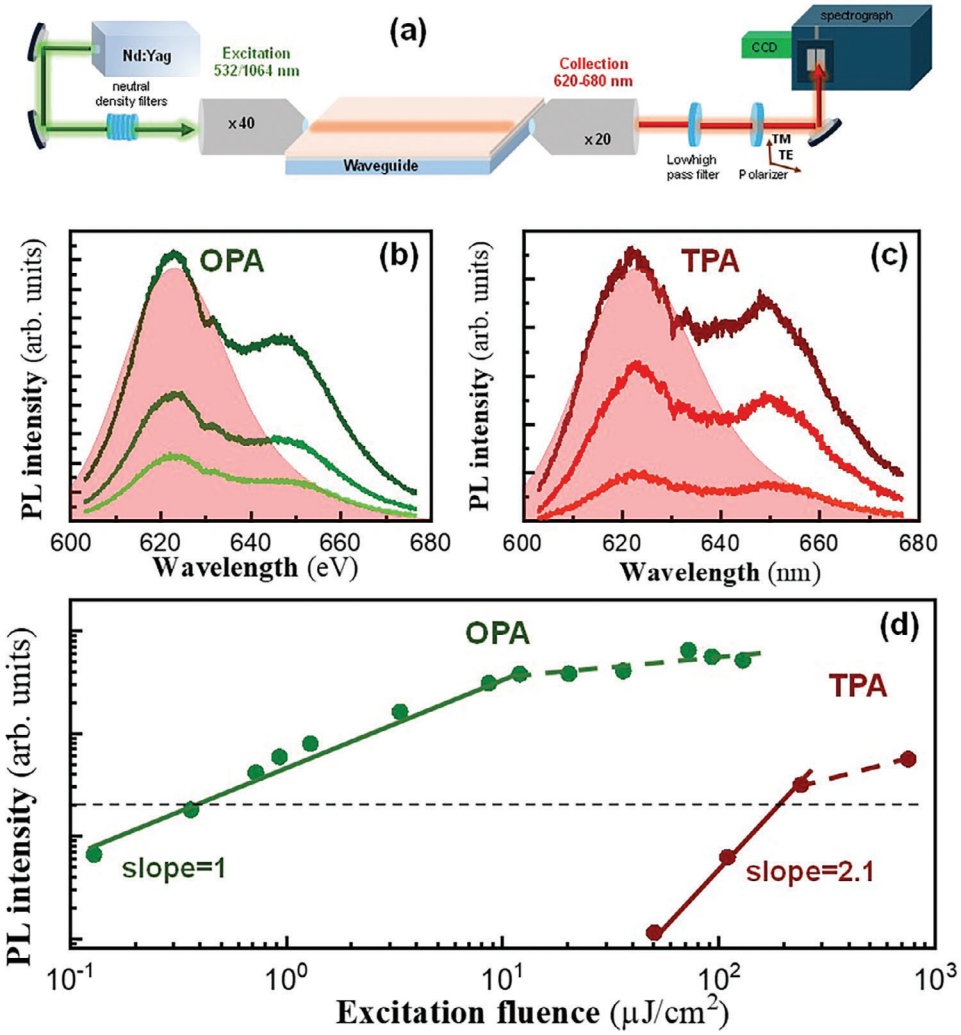

Figure 4. a) Experimental set-up used to characterize waveguided PL. b) Guided PL Spectra were obtained under OPA at 532 nm for different excitation powers. c) Guided PL spectra were obtained under TPA at 1064 nm for different excitation powers. d) Log–log plot of the PL intensity versus excitation measured under OPA (green symbols) and TPA (red symbols). Solid and dashed lines represent the slope of fitted data to a potential law and the saturation part, respectively. The Black dashed line indicates the number of photons from which the emission efficiency is calculated.

the waveguide geometry, we expect a stronger influence of these lower energy states in comparison to the case of backscattering geometry (red shaded area in Figure 4b), because of more efficient excitation of the borders and the added influence of self-absorption effects. Indeed, the TPA spectra collected at the output edge of the waveguide have a similar shape (reddish color lines under different excitation powers in Figure 4c) as that measured with ps pulses at 532 nm (Figure 4b), probably because these spectra correspond to the contribution of all grains excited along the length of the waveguide (1–2 mm), leading to an almost similar average. Accordingly, the dependence of the intensity of PL versus excitation follows a quadratic behavior ($I_{PL} \propto I^2$) characteristic of the nonlinear TPA,[56] see red symbols and slope in the log–log plot of Figure 4d, while the PL generated under OPA at 532 nm exhibits a linear slope ($I_{PL} \propto I$) characteristic from spontaneous emission, see green symbols and slope in the log–log plot of Figure 4d. Here, it is worth mentioning that PL under TPA is obtained above a threshold of 50 μJ cm^{-2}, which is ≈1 fold smaller than that reported for 3D $MAPbX_3$ perovskites or $CsPbX_3$ (X = Br, I) nanocrystals.[52] Besides, it is interesting to calculate the efficiency of emission under both excitation regimes. Considering an excitation fluence below the threshold of stimulated emission and saturation of Spontaneous emission, the number of electron-hole pairs photogenerated under OPA (n_{OPA}) and TPA (n_{TPA}) is given by $n_{OPA} = \alpha \cdot \varphi$ and $n_{TPA} = \beta \cdot \varphi^2 \cdot h\nu_{TPA}$, respectively,[56] where φ is the flux of incident photons (i.e., peak intensity divided by photon energy), α the linear absorption coefficient and β the nonlinear absorption coefficient. If the excitation is set below the black dashed line plotted in Figure 4d when crossing the corresponding I_{PL} versus power curves (0.4 and 200 μJ cm^{-2} for OPA and TPA, respectively), considering that $\alpha \approx 18$ μm^{-1} at 532 nm (Figure 1a) and $\beta = 8.5$ cm MW^{-1} at 1064 nm (Figure 2c), photogenerated carrier densities are $n_{OPA} \approx 2 \cdot 10^{17}$ cm^{-3} and $n_{TPA} \approx 9 \cdot 10^{17}$ cm^{-3} per pulse energy (2 ps in this case), which are below the Mott concentration reported for perovskite materials, $\approx 10^{18}$ cm^{-3}.[58]

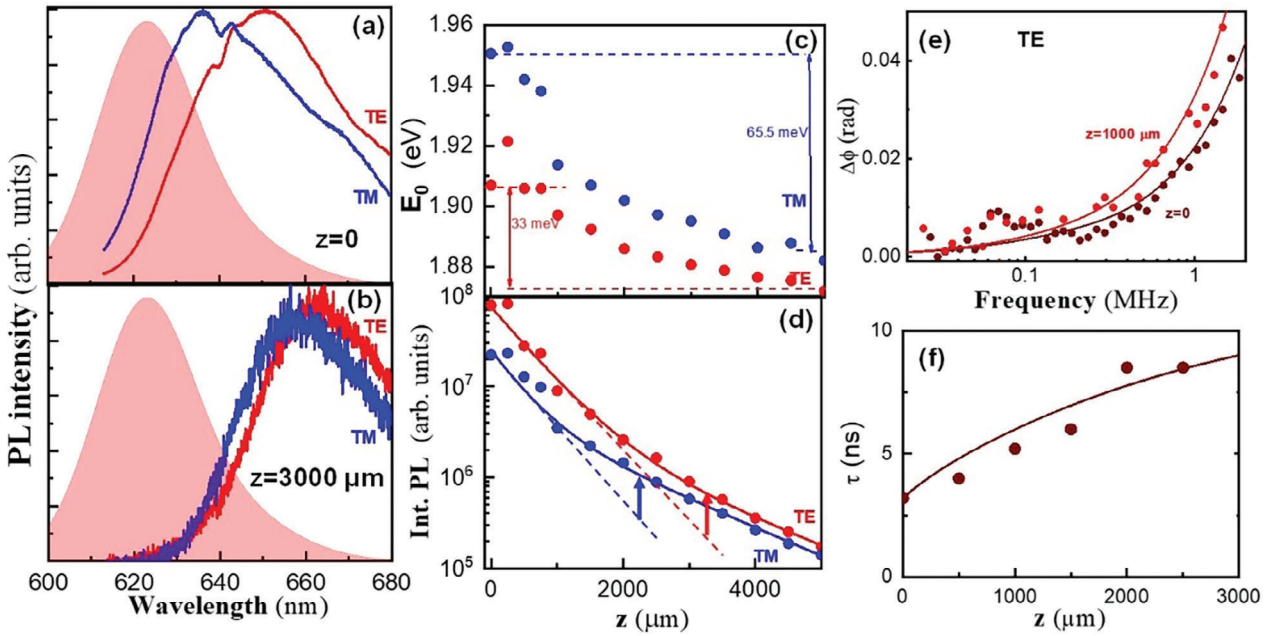

Figure 5. PL spectra were measured with the set-up illustrated in Figure S6 (Supporting Information) on a flexible substrate. a) Spectrum at z = 0 b) Spectrum at z = 3000 μm. c) Position of the peak as a function of z. d) Integrated intensity as a function of z. Characterization of PR by frequency modulated spectroscopy for TE polarization. e) Phase shift as a function of the modulated frequency. f) Decay time as a function of z. Red and blue colors refer to TE and TM polarization, respectively. Red area the spectrum measured under back scattering geometry.

Then, photons collected from photogenerated carriers by the two mechanisms, n_{OPA} and n_{TPA}, will be given by $n_{phOPA} = \eta_{OPA} \cdot n_{OPA}$ and $n_{phTPA} = 0.5 \cdot \eta_{TPA} \cdot n_{TPA}$, where η includes the efficiencies of emission and collection, and the factor of 0.5 comes by the two infrared photons needed to generate 1 PL photon. Considering the dashed line in Figure 4d, where $n_{phOPA} = n_{phTPA}$, the ratio of efficiencies by the TPA and OPA mechanisms becomes:

$$\frac{\eta_{TPA}}{\eta_{OPA}} = \frac{I_{OPA} \cdot \alpha}{I_{TPA}^2 \cdot \beta} \tag{2}$$

resulting $\eta_{TPA} = 0.02 \cdot \eta_{OPA}$. Since the collection efficiency is the same in both experiments, this number accounts for the internal efficiency generated in the waveguide. At a fluence of $9 \cdot 10^{15}$ cm^{-3}/pulse, the integrated intensity of the PL emitted under OPA conditions is estimated to be $8 \cdot 10^4$ photons/sec. If this intensity is generated in a waveguide slab of ≈100 nm (thickness of the film) x100 μm (width of the planar waveguide defined by the end-fire coupled excitation laser) x 1 mm (length of the waveguide) and a repetition rate of 100 Hz, the total efficiency of the OPA and TPA the device results in $9 \cdot 10^{-4}$% and $1.8 \cdot 10^{-5}$%, respectively. Of course, these are total efficiencies that account for the efficiency of photon extraction, the losses by Fresnel reflections in the lenses, and the losses in the monochromator. Considering a decoupling efficiency with the end-fire coupling technique of 1% that accounts for the Fresnel reflection and misalignment[61] and 10% of transmitted light through the slit of the spectrograph and the grating, the internal emission efficiencies of OPA and TPA processes become ≈0.9% and 0.018%, respectively.

2.5. Photon Recycling

The efficiency of PL emission along PEA_2SnI_4 waveguides can be further improved by effectively exploiting the important overlap of the absorption and emission characteristics of these materials, see Figure 1a.[13,34,37,47] Under a certain propagation of the PL along the films, such overlap will be giving several cycles of (re)absorption and (re)emission of photons from a primary excitation (electrical or optical injection) in the semiconductor. This process is called photon recycling (PR) because results in a population of recycled photons travelling through the material and with it an enhancement of the light signal and photogenerated carriers at propagating distances where any primary signal would be arriving if only one absorption-emission cycle would be taking place in the semiconductor. Thus, PR can be also considered as an optical gain mechanism that would enhance the performance of optoelectronic devices, such as solar cells or LEDs.[62,61] In particular, the waveguides proposed here are an ideal configuration to maximize the yield of this process, because of the high confinement of the fundamental modes, TE_0 and TM_0, at the PL wavelength in the semiconductor thin film (Figure 3c). Indeed, the demonstration of this mechanism in PEA_2SnI_4 is particularly beneficial for the implementation of red optical sources, as the material exhibits pure red emission, and the PR can introduce a gain mechanism to enhance the effective emission efficiency. At these conditions, photon recycling is studied here with the frequency-modulated technique described in detail elsewhere[44] and illustrated in Figure S6 (Supporting Information). The experiments carried out on rigid and flexible waveguides provide similar results, see Figures 5 and S7 (Supporting Information), respectively. **Figure** 5a shows a bright PL

Spectrum at z = 0 with a noticeable energy difference (35–40 meV) between the waveguided PL peak in TE and TM polarizations, which can be attributed to the anisotropy between electric field parallel and perpendicular to our multilayered 2D PEA_2SnI_4 films, which exhibited the preferential orientation (002) (Figure S2, Supporting Information).[24,63] At z = 3000 μm the PL spectra under both polarizations experience a noticeable redshift characteristic of the PR effect, ΔE, see Figure 5b. This redshift depends on the overlap of PL and absorption spectra and increases with the propagation distance (z), as shown in Figure 5c. In particular, ΔE reaches ≈40 meV and ≈65 meV for TE (red symbols) and TM (blue symbols) polarizations, respectively. The dependence of PL intensity as a function of z is shown in Figure 5d (red and blue solid circles for TE and TM polarizations, respectively), can be fitted with a two exponential decay function (see supporting information), solid lines in Figure 5d, with two characteristic propagation lengths of 140–150 and 400–500 μm, which are slightly shorter than those obtained in previously studied films formed by $CsPbBr_3$ nanocrystals.[44] The first exponential decay is attributed to the propagation of primary photons averaged over the whole PL spectra, and the second (and longer) propagation length is ascribed to the compensation of losses by the PR effect, where the secondary photon flux results iin an effective gain assisted mechanism for the emitted PL. This effective gain can be estimated by the ratio of the experimental PL intensity at a given distance and the corresponding PL intensity that would be active with only the first decay at the same propagation distance, see prolongated slope with the dashed lines in Figure 5d. For example, at the propagation distance z = 3000 μm, the effective gain reaches a factor ≈4 for TE polarization (see arrows in Figure 5d). Here, it is necessary to emphasize that the comparable performances obtained for devices fabricated on flexible, Figure 5, and rigid substrates, see Figure S7 (Supporting Information), represent an important result toward the implementation of a flexible technology based on lead-free perovskites. Although flexible substrates usually introduce dislocations that degrade the figures of merit of the final device, in this case, both rigid and flexible waveguides exhibited similar parameters, such as the red shift after propagation in the waveguide (≈65 meV in TE and ≈40 meV in TM) and a comparable level of the decoupled signal, indicating similar propagation losses.

Our modulated frequency technique (using a frequency-modulated laser up to 2 MHz) is suitable to evaluate the influence of the PR effect in the effective exciton recombination rate because we can determine PL decay time constants between 1 ns and several μs by analyzing the phase-shift of the collected modulated PL, see supporting information. The dependence of the PL intensity as a function of the modulation frequency, see Figure 5e reveals an increase of the effective recombination time from 3 to 8.5 ns, when the recycled photons travel 3 mm of distance along the waveguide, as shown in Figure 5f. In our previous work developed on waveguides based on films made of perovskite $CsPbBr_3$ nanocrystals, where carrier transport is absent, we concluded the strong directionality of the PR propagation due to the light confinement in the waveguide, which introduces a ″photon drift″ added to the known diffusive term of the PR effect that reduces significantly the “slowing down” of the recombination to the range of 4–5 ns in 3 mm.[44] In the present case, where the waveguide integrates a polycrystalline 2D perovskite, the effective recombination time increases a similar quantity along a similar propagation distance, see Figure 5f, which agrees with the effective gain deduced in Figure 5d. However, we observe a simultaneous strong intensity decrease with z (shorter propagation distances as compared to what we measured in films of $CsPbBr_3$ nanocrystals), suggesting some loss of directionality (drift) in the PR-light propagation, which is attributed here to the exciton diffusion in the polycrystalline film together with more important nonradiative losses, as already deduced from the relatively low PL QY given above.

3. Conclusion

To conclude, lead-free 2D PEA_2SnI_4 polycrystalline thin films were successfully incorporated in polymer waveguides. This material is a 2D semiconductor with outstanding optical properties, such as high absorption, anisotropy in the emission spectra, and high nonlinear optical parameters, which were fully characterized. Particularly, PEA_2SnI_4 exhibited giant linear and nonlinear absorption coefficients: $\alpha > 10^5$ cm^{-1} and β = 7–10 cm MW^{-1}, with an outstanding nonlinear refractive index n_2 = 1.5–4 cm^2 GW^{-1}. Therefore, PEA_2SnI_4, as surely other 2D tin perovskite semiconductors formed with long organic cations, are excellent candidates to develop different linear and nonlinear photonic devices combining their high linear absorption efficiency and nonlinear optical coefficients. Accordingly, the performance of optical waveguides integrating this 2D semiconductor was studied, making it possible to generate and guide PL under one- and two-photon absorption excitation conditions and demonstrated a propagation enhancement by photon recycling. In fact, PL under TPA is obtained with excitation fluences as low as 50 μJ cm^{-2}, whereas recycled photons travel over distances longer than 3 mm, as characterized by an increased average lifetime from 3 to 8.5 ns, which can be used for improving emitting devices with an appropriate geometrical design. In spite of the reported potentiality of 2D tin perovskites in photonics, still needed a reduction of nonradiative channels, most probably related to Sn^{+4} defects at surface and grain boundaries, in order to make possible the amplification of the spontaneous emission and lasing at room temperature, as already demonstrated in the case of $(3T)_2MA_1Sn_nI_7$ [3T: 2-([2,2′:5′,2″-terthiophen]-5-yl)ethan-1-aminium],[38] even if still needed high excitation fluences (374 μJ cm^{-2}).

4. Experimental Section

Materials: Tin(II) iodide (SnI_2, 99.99%), tin(II) fluoride (SnF_2, 99%), Sodium borohydride ($NaBH_4$, 96%), Poly-methyl methacrylate (PMMA,99.9%), N, N-dimethylformamide (DMF, 99.8%), and dimethylsulfoxide (DMSO, 99.8%) were purchased from Sigma-Aldrich. Phenylethylammonium iodide (PEAI 98%) was purchased from Greatcell solar materials. All materials were used as received with no further purifications.

Perovskite Solution Preparation: 0.8 M perovskite precursor solution was prepared by dissolving stoichiometric PEAI and SnI_2 in a solvent mixture of DMF:DMSO (4:1) and stirred at room temperature overnight. For the solutions containing additives, SnF_2 (0.08 M) and/or $NaBH_4$ (2 mM), were added to the precursor solutions during the preparation.

Fabrication of Thin Films: The perovskite precursor solution of PEA_2SnI_4 was deposited on the borosilicate, Si/SiO_2, glass, or flexible

Polyethylene Terephthalate (PET) substrates by spin-coating at 4000 rpm and 800 of acceleration for 50 s, afterward a two-step annealing was performed at 65 and 90 °C for 1 and 15 min, respectively. Prior to the deposition, the substrates were cleaned with ethanol, acetone, and isopropanol, respectively, in an ultrasonic bath for 15 min each; after the cleaning procedure, they were dried with N_2. Before the active layer deposition, the substrates were treated with UV-Ozone for 10 min, then the samples were transferred to an N_2 filled glovebox for the perovskite film deposition. Finally, after the substrates were cooled down at room temperature, the Sn-perovskite film was covered with 0.7–1 µm of Poly(methyl methacrylate) (PMMA) to define waveguides and certain protection against ambient conditions.

Absorption and PL: The reflectance and transmittance of PEA_2SnI_4 films were measured by a commercial reflectometer (NanoCalc-2000 from Mikropack) to extract the complex refractive index of the film. PL and Time-Resolved PL (TRPL) were characterized with the use of an FLS1000 PL spectrometer (Edinburgh Instruments) with excitation and detection double monochromators. The spectrally selected PL light was detected with a high-speed PMT in a cooled housing with an instrument response of ≈200 ps coupled with a photon-counting system. A 150 W Ozone-free xenon arc lamp was used as a light source for steady-state measurements and a pulsed 405 nm solid-state laser with a pulse duration of ≈1 ns for TRPL measurements. Decay times were obtained by convoluting the instrument response with a biexponential decay function.

PL Under two Photon Absorption: PL was measured in transmission geometry by using as excitation a Nd:Yag pulsed laser (1064 nm, 1 ns, 20 KHz) and collecting the generated PL in spin-coated films prepared on a borosilicate substrate.

Nonlinear Optical Parameters: Nonlinear optical parameters were obtained by using the Z-scan geometry using the aforementioned 1064 nm Nd:YAG pulsed laser. The excitation beam was focused into an 11–13 µm spot with the aid of a 25 mm focal lens in order to keep a Rayleigh length (close to 350 µm) much longer than the thickness of the sample (500 nm). Then, the light transmitted through the film deposited on borosilicate was collected with a 100 mm focal lens to a Thorlabs CCD DCU224 M camera, while the sample holder was translated with a Thorlabs MTS25A-Z8 platform. The camera recorded one image for each translation step (z) to extract the nonlinear parameters with the analysis of the beam intensity profile following the procedure explained elsewhere.[52]

Waveguide Characterization: Waveguides were characterized by end-fire coupling a Nd:YAG laser at 532 nm/1064 nm (2-ps pulses at 100 Hz repetition rate, FYLA) at the input edge of the sample (PEA_2SnI_4 films deposited on Si/SiO_2 and PET substrates) with the aid of a 40x microscope objective mounted on a XYZ stage. The intensity of the excitation beam was controlled by neutral density filters. Waveguided PL was collected at the output edge of the sample with a 20x microscope objective, also mounted on the XYZ stage. The outcoupled PL signal was collected, after 550 nm/1000 nm long/short pass filters and a linear polarizer, with the aid of a cylindrical lens and dispersed by a grating spectrograph (DNS-300 from DeltaNu) and detected by a back-illuminated Si CCD (DV420A-OE from Andor) at its exit. Photon Recycling was studied in the waveguides with the experimental set-up described in detail elsewhere.[44] As a summary, the thin film waveguide was excited at 450 nm (MDL-XS-450, CNI laser) with a modulated beam (25 kHz to 1 MHz) from the surface with the aid of a cylindrical lens that focused the beam on an 800 × 200 µm stripe. Then, the PL was collected from the output edge as a function of the distance between the excitation and the edge of the sample (z) and analyzed by the same grating spectrograph described above. Besides, the frequency domain spectroscopy of the waveguided PL was carried out under synchronous detection with a Si Avalanche Photodetector (APD120A/M, Thorlabs) connected to a high-frequency lock-in amplifier (SR844, Stanford Research Systems).

Supporting Information

Supporting Information is available from the Wiley Online Library or from the author.

Acknowledgements

This project received funding from the European Union's Horizon 2020 research and innovation programme under grant agreement No. 862656 (project DROP-IT), by the Spanish MINECO through projects no. PID2020-120484RB-I00 and PID2022-140090OB-C21 (PLEDs project), and by Generalitat Valenciana project IDIFERER 2020–064. This study also forms part of the Advanced Materials (project no. MFA/2022/020) and Quantum Communication programmes (project no. COMCUANTICA/009) and was supported by MCIN with funding from European Union NextGenerationEU (PRT-RC17.11) and by Generalitat Valenciana.

Conflict of Interest

The authors declare no conflict of interest.

Data Availability Statement

The data that support the findings of this study are available from the corresponding author upon reasonable request.

Keywords

nonlinear, PEA2SnI4, photon recycling, two photon absorption, waveguide

Received: September 2, 2024
Revised: November 8, 2024
Published online: November 29, 2024

[1] Q. Chen, N. De Marco, Y. (Michael) Yang, T.-B. Song, C.-C. Chen, H. Zhao, Z. Hong, H. Zhou, Y. Yang, *Nano Today* **2015**, *10*, 355.
[2] H. Zhu, Y. Fu, S. Jin, M. P. Hautzinger, J. Chen, X.-Y. Zhu, *Nat. Rev. Mater.* **2019**, *4*, 169.
[3] W. Li, Z. Wang, F. Deschler, S. Gao, R. H. Friend, A. K. Cheetham, *Nat. Rev. Mater.* **2017**, *2*, 16099.
[4] Z. Shi, A. H. Jayatissa, *Materials (Basel)* **2018**, *11*, 729.
[5] F. P. García De Arquer, A. Armin, P. Meredith, E. H. Sargent, *Nat. Rev. Mater.* **2017**, *2*, 16100.
[6] Q. Zhang, R. Su, W. Du, X. Liu, L. Zhao, S. T. Ha, Q. Xiong, *Small Methods* **2017**, *1*, 1700163.
[7] W. F. Yang, F. Igbari, Y. H. Lou, Z. K. Wang, L. S. Liao, *Adv. Energy Mater.* **2020**, *10*, 1902584.
[8] I. López-Fernández, D. Valli, C. Y. Wang, S. Samanta, T. Okamoto, Y. T. Huang, K. Sun, Y. Liu, V. S. Chirvony, A. Patra, J. Zito, L. De Trizio, D. Gaur, H. T. Sun, Z. Xia, X. Li, H. Zeng, I. Mora-Seró, N. Pradhan, J. P. Martínez-Pastor, P. Müller-Buschbaum, V. Biju, T. Debnath, M. Saliba, E. Debroye, R. L. Z. Hoye, I. Infante, L. Manna, L. Polavarapu, *Adv. Funct. Mater.* **2024**, *34*, 2307896.
[9] J. Zhou, J. Luo, X. Rong, P. Wei, M. S. Molokeev, Y. Huang, J. Zhao, Q. Liu, X. Zhang, J. Tang, Z. Xia, *Adv. Opt. Mater.* **2019**, *7*, 1900139.
[10] D. Shao, W. Zhu, G. Xin, X. Liu, T. Wang, S. Shi, J. Lian, S. Sawyer, *J. Mater. Chem. C* **2020**, *8*, 1819.
[11] H. Zhu, W. Yang, Y. Reo, G. Zheng, S. Bai, A. Liu, Y. Y. Noh, *Nat. Electron.* **2023**, *6*, 650.
[12] J. M. Heo, H. Cho, S. C. Lee, M. H. Park, J. S. Kim, H. Kim, J. Park, Y. H. Kim, H. J. Yun, E. Yoon, D. H. Kim, S. Ahn, S. J. Kwon, C. Y. Park, T. W. Lee, *ACS Energy Lett.* **2022**, *7*, 2807.
[13] G. Vescio, J. Sanchez-Diaz, J. L. Frieiro, R. S. Sánchez, S. Hernández, A. Cirera, I. Mora-Seró, B. Garrido, *ACS Energy Lett.* **2022**, *7*, 3653.
[14] D. Han, J. Wang, L. Agosta, Z. Zang, B. Zhao, L. Kong, H. Lu, I. Mosquera-Lois, V. Carnevali, J. Dong, J. Zhou, H. Ji, L. Pfeifer, S. M.

Zakeeruddin, Y. Yang, B. Wu, U. Rothlisberger, X. Yang, M. Grätzel, N. Wang, *Nature* **2023**, *622*, 493.
[15] J. Sanchez-Diaz, R. S. Sánchez, S. Masi, M. Krecmarová, A. O. Alvarez, E. M. Barea, J. Rodriguez-Romero, V. S. Chirvony, J. F. Sánchez-Royo, J. P. Martinez-Pastor, I. Mora-Seró, *Joule* **2022**, *6*, 861.
[16] Y. Shi, Z. Zhu, D. Miao, Y. Ding, Q. Mi, *ACS Energy Lett.* **2024**, *9*, 1895.
[17] G. Xing, M. H. Kumar, W. K. Chong, X. Liu, Y. Cai, H. Ding, M. Asta, M. Grätzel, S. Mhaisalkar, N. Mathews, T. C. Sum, *Adv. Mater.* **2016**, *28*, 8191.
[18] I. Suárez, V. S. Chirvony, J. Sánchez-Díaz, R. S. Sánchez, I. Mora-Seró, J. P. Martínez-Pastor, *Adv. Opt. Mater.* **2022**, *10*, 2200458.
[19] H. P. Adl, J. Sánchez-Díaz, G. Vescio, A. Cirera, B. Garrido, F. A. V. Pacheco, W. Żuraw, Ł. Przypis, S. Öz, I. Mora-Seró, J. P. Martínez-Pastor, I. Suárez, *Adv. Mater.* **2024**, *36*, 2313252.
[20] V. S. Chirvony, I. Suárez, J. Sanchez-Diaz, R. S. Sánchez, J. Rodríguez-Romero, I. Mora-Seró, J. P. Martínez-Pastor, *Adv. Mater.* **2023**, *35*, 2208293.
[21] X. Gao, X. Zhang, W. Yin, H. Wang, Y. Hu, Q. Zhang, Z. Shi, V. L. Colvin, W. W. Yu, Y. Zhang, *Adv. Sci.* **2019**, *6*, 1900941.
[22] J. Hu, L. Yan, W. You, *Adv. Mater.* **2018**, *30*, 1802041.
[23] C. Ge, E. M. Hutter, D. H. Cao, N. Renaud, C. C. Stoumpos, J. T. Hupp, T. J. Savenije, M. G. Kanatzidis, F. C. Grozema, *J. Phys. Chem. C* **2017**, *121*, 18674.
[24] J. Li, J. Ma, X. Cheng, Z. Liu, Y. Chen, D. Li, *ACS Nano* **2020**, *14*, 2156.
[25] H. Tsai, W. Nie, C. C. Stoumpos, L. Pedesseau, C. Katan, M. Kepenekian, C. M. M. Soe, K. Appavoo, M. Y. Sfeir, S. Tretiak, P. M. Ajayan, M. G. Kanatzidis, J. Even, J. J. Crochet, A. D. Mohite, *Science* **2017**, *1292*, 1288.
[26] X. K. Liu, F. Gao, *J. Phys. Chem. Lett.* **2018**, *9*, 2251.
[27] F. O. Saouma, C. C. Stoumpos, J. Wong, M. G. Kanatzidis, J. I. Jang, *Nat. Commun.* **2017**, *8*, 742.
[28] M. Ren, S. Cao, J. Zhao, B. Zou, R. Zeng, *Advances and Challenges in Two-Dimensional Organic–Inorganic Hybrid Perovskites Toward High-Performance Light-Emitting Diodes*, Springer, Singapore **2021**.
[29] H. Tsai, W. Nie, J. C. Blancon, C. C. Stoumpos, C. M. M. Soe, J. Yoo, J. Crochet, S. Tretiak, J. Even, A. Sadhanala, G. Azzellino, R. Brenes, P. M. Ajayan, V. Bulović, S. D. Stranks, R. H. Friend, M. G. Kanatzidis, A. D. Mohite, *Adv. Mater.* **2018**, *30*, 1704217.
[30] L. Zhang, C. Sun, T. He, Y. Jiang, J. Wei, Y. Huang, M. Yuan, *Light Sci. Appl.* **2021**, *10*, 61.
[31] M. Y. Chen, J. T. Lin, C. S. Hsu, C. K. Chang, C. W. Chiu, H. M. Chen, P. T. Chou, *Adv. Mater.* **2018**, *30*, 1706592.
[32] S. Sui, J. Zhou, A. Wang, G. Hu, W. Meng, C. Wang, Y. Liu, J. Wu, Z. Deng, *Nanoscale Adv* **2021**, *3*, 3875.
[33] H. Liang, F. Yuan, A. Johnston, C. Gao, H. Choubisa, Y. Gao, Y. K. Wang, L. K. Sagar, B. Sun, P. Li, G. Bappi, B. Chen, J. Li, Y. Wang, Y. Dong, D. Ma, Y. Gao, Y. Liu, M. Yuan, M. I. Saidaminov, S. Hoogland, Z. H. Lu, E. H. Sargent, *Adv. Sci.* **2020**, *7*, 1903213.
[34] F. Yuan, X. Zheng, A. Johnston, Y. Wang, C. Zhou, Y. Dong, B. Chen, H. Chen, J. Z. Fan, G. Sharma, P. Li, Y. Gao, O. Voznyy, H. Kung, Z. Lu, O. M. Bakr, E. H. Sargent, *Sci. Adv.* **2020**, *6*, eabb0253.
[35] T. Zhang, C. Zhou, X. Feng, N. Dong, H. Chen, X. Chen, L. Zhang, J. Lin, J. Wang, *Nat. Commun.* **2022**, *13*, 60.
[36] K. R. Yun, T. J. Lee, S. K. Kim, J. H. Kim, T. Y. Seong, *Adv. Opt. Mater.* **2023**, *11*, 2201974.
[37] S. Cai, Y. Ju, Y. Wang, X. Li, T. Guo, H. Zhong, L. Huang, *Adv. Sci.* **2022**, *9*, 2104708.
[38] Y. Li, H. Zhou, M. Xia, H. Shen, T. Wang, H. Gao, X. Sheng, Y. Han, Z. Chen, L. Dou, H. Zhu, E. Shi, *Sci. Adv.* **2023**, *9*, eadh0517.
[39] A. L. Alvarado-Leaños, D. Cortecchia, C. N. Saggau, S. Martani, G. Folpini, E. Feltri, M. D. Albaqami, L. Ma, A. Petrozza, *ACS Nano* **2022**, *16*, 20671.
[40] A. Ferrando, J. P. Martínez Pastor, I. Suárez, *J. Phys. Chem. Lett.* **2018**, *9*, 5612.
[41] I. Suárez, J. P. Martínez-Pastor, M. F. Oszajca, N. A. Lüchinger, B. Graves, S. Agouram, C. Milián, A. Ferrando, *Adv. Opt. Mater.* **2023**, *11*, 2202120.
[42] A. Mushtaq, B. Pradhan, D. Kushavah, Y. Zhang, M. Wolf, N. Schrenker, E. Fron, S. Bals, J. Hofkens, E. Debroye, S. K. Pal, *ACS Photonics* **2021**, *8*, 3365.
[43] D. Liu, J. Liu, K. Zhang, P. Wang, C. Miao, J. Sun, B. Zhang, J. He, X. Hao, Z. X. Yang, *J. Phys. Chem. C* **2021**, *125*, 803.
[44] J. Navarro-Arenas, I. Suárez, A. F. Gualdrón-reyes, I. Mora-seró, J. Bisquert, J. Martínez, *Adv. Opt. Mater.* **2021**, *9*, 2100807.
[45] S. De Wolf, J. Holovsky, S. J. Moon, P. Löper, B. Niesen, M. Ledinsky, F. J. Haug, J. H. Yum, C. Ballif, *J. Phys. Chem. Lett.* **2014**, *5*, 1035.
[46] D. Ritter, K. Weiser, *Opt. Commun.* **1986**, *57*, 336.
[47] Y. Ju, X. gang Wu, S. Huang, G. Dai, T. Song, H. Zhong, *Adv. Funct. Mater.* **2022**, *32*, 2.
[48] J. Navarro-Arenas, I. Suárez, V. S. Chirvony, A. . Gualdrón-Reyes, I. Mora-Seró, J. P. Martínez-Pastor, *J. Phys. Chem. Lett.* **2019**, *10*, 6389.
[49] B. Song, J. Hou, H. Wang, S. Sidhik, J. Miao, H. Gu, H. Zhang, S. Liu, Z. Fakhraai, J. Even, J. C. Blancon, A. D. Mohite, D. Jariwala, *ACS Mater. Lett.* **2021**, *3*, 148.
[50] G. Lifante, *Integrated Photonics : Fundamentals*, Wiley, Hoboken, New Jersey, US **2002**.
[51] K. M. Islam, R. Synowicki, T. Ismael, I. Oguntoye, N. Grinalds, M. D. Escarra, *Adv. Photonics Res.* **2021**, *2*, 2000180.
[52] I. Suárez, M. Vallés-Pelarda, A. F. Gualdrón-Reyes, I. Mora-Seró, A. Ferrando, H. Michinel, J. R. Salgueiro, J. P. M. Pastor, *APL Mater.* **2019**, *7*, 041106.
[53] X. Han, Y. Zheng, S. Chai, S. Chen, J. Xu, *Nanophotonics* **2020**, *9*, 1787.
[54] I. Abdelwahab, G. Grinblat, K. Leng, Y. Li, X. Chi, A. Rusydi, S. A. Maier, K. P. Loh, *ACS Nano* **2018**, *12*, 644.
[55] W. Liu, J. Xing, J. Zhao, X. Wen, K. Wang, P. Lu, Q. Xiong, *Adv. Opt. Mater.* **2017**, *5*, 1601045.
[56] J. Chen, W. Zhang, T. Pullerits, *Mater. Horiz.* **2022**, *9*, 2255.
[57] J. Wang, Y. Mi, X. Gao, J. Li, J. Li, S. Lan, C. Fang, H. Shen, X. Wen, R. Chen, X. Liu, T. He, D. Li, *Adv. Opt. Mater.* **2019**, *7*, 1900398.
[58] I. Suárez, E. J. Juárez-Pérez, V. S. Chirvony, I. Mora-Seró, J. P. Martínez-Pastor, *Phys. Rev. Appl.* **2020**, *13*, 064071.
[59] I. Suárez, E. Hassanabadi, A. Maulu, N. Carlino, C. A. Maestri, M. Latifi, P. Bettotti, I. Mora-Seró, J. P. Martínez-Pastor, *Adv. Opt. Mater.* **2018**, *6*, 1800201.
[60] V. S. Chirvony, G. Muñoz-Matutano, I. Suárez, G. Vescio, D. N. Dirin, M. V. Kovalenko, B. Garrido, A. Cirera, J. P. Martínez-Pastor, *Adv. Funct. Mater.* **2024**, *34*, 2405154.
[61] C. Cho, B. Zhao, G. D. Tainter, J. Lee, D. Di, F. Deschler, N. C. Greenham, R. H. Friend, *Nat. Commun.* **2020**, *11*, 611.
[62] A. R. Bowman, M. Anaya, N. C. Greenham, S. D. Stranks, *Phys. Rev. Lett.* **2020**, *125*, 67401.
[63] I. Suárez, R. Muñoz, V. Chirvony, M. Artemyev, A. Prudnikau, A. Mikhailov, *IEEE J. Sel. Top. Quantum Electron.* **2012**, *23*, 4400408.